RSC Advances

PAPER

View Article Online
View Journal | View Issue



Cite this: *RSC Adv.*, 2018, **8**, 42398

# Chemical solution deposition of $Y_{1-x}Gd_xBa_2Cu_3O_{7-\delta}$–$BaHfO_3$ nanocomposite films: combined influence of nanoparticles and rare-earth mixing on growth conditions and transport properties

Pablo Cayado,* Manuela Erbe, Sandra Kauffmann-Weiss, Alexandra Jung, Jens Hänisch and Bernhard Holzapfel

$Y_{1-x}Gd_xBa_2Cu_3O_{7-\delta}$–$BaHfO_3$ (YGBCO–BHO) nanocomposite films containing 12 mol% BHO nanoparticles and different amounts of Gd were prepared by chemical solution deposition following the trifluoroacetic route on $SrTiO_3$ single crystals in order to study the influence of the rare earth stoichiometry on structure, morphology and superconducting properties of these films. We optimized the growth process for each of several Gd contents of the 220 nm thick YGBCO–BHO films by varying crystallization temperature and oxygen partial pressure. This optimization process led to the conclusion that mixing the rare earths in YGBCO–BHO films leads to wider growth parameter windows compared to YBCO-BHO and GdBCO-BHO films giving larger freedom for selecting the most convenient processing parameters in order to adapt to different substrates or applications which is very important for the industrial production of coated conductors. The optimized films show a continuous increase of $T_c$ with Gd content $x$ from ~90 K for the YBCO-BHO films to ~94 K for the GdBCO-BHO films. Consequently, an increase of the 77 K self-field $J_c$ with Gd content is observed reaching values > 7 MA cm$^{-2}$ for Gd contents $x$ > 0.5. The transport properties of these films under applied magnetic fields are significantly improved with respect to the pristine YBCO films. All YGBCO–BHO nanocomposite films grew epitaxially with $c$-axis orientation and excellent out-of-plane and in-plane texture. The films are dense with a low amount of pores and only superficial indentations.

Received 6th November 2018
Accepted 11th December 2018

DOI: 10.1039/c8ra09188a

rsc.li/rsc-advances



## 1 Introduction

Research on high-temperature superconductors (HTS) has become one of the most active topics in the field of applied superconductivity. Nowadays, most of the studies in this area are focused on $REBa_2Cu_3O_{7-\delta}$ (REBCO, RE = Rare Earth) compounds. Their properties, especially their high critical temperature ($T_c$) and high current carrying capability even at high fields, make them attractive particularly for power applications. Therefore, they are the base material for the fabrication of second-generation high-$T_c$ superconducting tapes, called Coated Conductors (CCs), which have promising perspectives for their use in multiple applications such as motors, generators and cables.[1–4]

Within this group of REBCO compounds, $YBa_2Cu_3O_{7-\delta}$ (YBCO) is the best known compound since it was the first superconductor that showed a critical temperature higher than the boiling point of liquid nitrogen ($LN_2$ 77 K). However, other REBCO compounds have attracted the attention of the community because they could exhibit better properties than YBCO.[5–9] These improvements in the properties are caused by variations in the electronic structures, valence states and the ionic radii of the rare earth (RE) atoms within the structures.[10–13] Although some of these REBCO compounds show better transport properties than YBCO, their synthesis may be much more complicated. This is because on the one hand the large RE ions, like $Nd^{3+}$ or $Sm^{3+}$, tend to partially substitute the $Ba^{2+}$ ions, and on the other hand the small RE ions, such as $Yb^{3+}$ and $Lu^{3+}$, do not fit properly into the according lattice site. Both facts cause the stability of the REBCO phase to decrease drastically.[5,10,14,15]

In order to partially overcome the difficulties in the synthesis of these single-large-ion REBCO compounds and at the same time improving the superconducting properties of the films, there is the possibility to mix different $RE^{3+}$ ions. By doing this, it seems possible to combine the phase diagrams of both individual compounds by enlarging the processing window in which high-quality epitaxial films are achievable. Moreover, in these mixed REBCO compounds studied in previous years in multiple

*Karlsruhe Institute of Technology (KIT), Institute for Technical Physics (ITEP), Hermann-von-Helmholtz-Platz 1, 76344 Eggenstein-Leopoldshafen, Germany. E-mail: pablo.cayado@kit.edu*

combinations of ions such as Y/Sm,[13,16,17] Y/Gd,[17,18] Y/Pr,[19–21] Y/Eu/Gd[22] or Nd/Eu/Gd,[23,24] the superconducting transport properties are improved due to enhanced flux pinning by the RE mixing itself. This improvement of the superconducting properties comes from the fact that the introduction of different elements in the lattice structure of a certain REBCO compound changes the properties of very localized areas in and around the dopants, which enhances the pinning force densities of the resulting system. This elemental substitution on the ionic sites of the RE unit cell causes both localized and macroscopic structures that are partially or fully non-superconducting, depending on variables such as the molar fraction of the substitution, chemical element, and others.[25,26] The improvement in the superconducting properties will depend on whether the RE elements are uniformly dispersed, or if segregation and/or coalescence of alternate-phase materials occurs throughout the composite. However, both cases might be beneficial. If the RE elements disperse homogeneously in the structure causing chemical substitutions, $T_c$ is affected in very localized regions around the doped areas. Therefore, fluctuations of $T_c$ are expected improving the pinning properties. On the other hand, if different clusters are formed, microscopic strain will be created in the vicinity of the different REBCO clusters which will also enhance the pinning properties of the films.[25]

Apart from that and in order to further improve the pinning properties in such films, secondary phases are introduced creating REBCO nanocomposites. This has been extensively investigated by many groups showing that the in-field transport properties of REBCO films can be vastly improved by both the "*in situ*" and the "*ex situ*" particle formation approaches.[27–32]

In the present study, we investigate the interplay between and combined effects of RE mixing and nanoparticle inclusion. We prepared mixed films containing $Y^{3+}$ and $Gd^{3+}$ ions to obtain YGBCO films since this combination has already been prepared in the past by chemical routes and Pulsed Laser Deposition (PLD) with excellent properties both on single crystals and buffered metallic tapes.[17,22,33,34] The samples in this work were prepared by Chemical Solution Deposition (CSD) which is a scalable and low-cost technique for the preparation of CCs.[35–38] In particular, we followed the well-known TFA-MOD (Trifluoroacetate-Metal–Organic Decomposition) route.[39] This route has already shown promising properties for YGBCO films,[17,22] but still the effort is not comparable to YBCO or GdBCO and so there is room for improvement, as we will demonstrate below. As nanoparticles (NPs) we used $BaHfO_3$ (BHO) prepared by the *in situ* formation approach in which the NPs are spontaneously segregated in the superconductor matrix during the growth process, a strategy that has already shown excellent results, as reported previously *e.g.* by our group.[9,30]

# 2 Sample preparation and characterization techniques

## 2.1 Sample preparation

The preparation method for the nanocomposite TFA solution is as described in ref. 9. First, two different solutions are prepared: YBCO with 12 mol% BHO and GdBCO with 12 mol% BHO (12% BHO from now on). For this, Y or Gd, Ba and Cu acetates of the RE, Ba, and Cu (purity > 99.99%, Alfa Aesar) as well as hafnium(IV) 2,4-pentanedionate ($Hf(acac)_4$) (97+%, Alfa Aesar) were weighed out and mixed to give a stoichiometric 1 : 2 : 3 ratio of the metal cations and 12 mol% BHO with respect to the RE, in deionized water. Then, an excess of trifluoroacetic acid (TFAH, 99.5+%, Alfa Aesar) was added to convert the acetates into trifluoroacetates. The remaining water and other impurities are removed by a rotary evaporator resulting in a highly viscous residue that is re-diluted in absolute methanol (99.9%). In order to further reduce the undesired remaining water, methanol is evaporated again several times in vacuum. The final concentration of 0.25 mol $l^{-1}$ in Y or Gd is adjusted with anhydrous methanol ending with a dark blue solution. The YGBCO + 12% BHO solutions are then made by mixing the initial YBCO + 12% BHO and GdBCO + 12% BHO solutions in different ratios obtaining the desired stoichiometry.

The approximately 220 nm thick YGBCO + 12% BHO films were prepared, firstly, by depositing the precursor solutions on $10 \times 10$ $mm^2$ (001)-oriented $SrTiO_3$ (STO) single crystals *via* spin coating (6000 rpm for 30 s for the STO). The subsequent "standard" pyrolysis and growth processes are described in ref. 40. The modifications to the "standard" growth process that lead to the presented results will be discussed in detail later. For electrical transport measurements, 10–20 μm wide microbridges were prepared by photolithography and wet-chemical etching.

## 2.2 Thin film characterization

The microstructure and phase purity of the films were investigated by X-ray diffraction (XRD) using a Bruker D8 diffractometer with CuKα radiation in Bragg–Brentano geometry. The surface morphology was analyzed by a LEO 1530 scanning electron microscope (SEM) with field emission gun (0.1 kV and 30 kV) by Zeiss. The self-field critical current density, $J_c^{sf}$, at 77 K was measured inductively with a Cryoscan (Theva, 50 μV criterion). Critical temperature $T_c$ and critical current densities $J_c$ were determined by transport measurements in 4-point geometry at a 14-T Quantum Design Physical Property Measurement System (PPMS). $T_c$ is defined as the temperature $T_{c,90}$ at which the resistance is 90% of the value above the transition. $J_c$ was determined *via* $V(I)$ curves by an electrical field criterion of 1 μV $cm^{-1}$.

# 3 Results and discussion

## 3.1 Optimization of growth process

The optimal growth conditions depend strongly on the (mean) RE size.[12,13] Therefore, the growth process had to be optimized for each Gd content $x$, where the previous reports of our group on the optimization of YBCO + 12% BHO and GdBCO + 12% BHO films using the same type of solutions served as ref. 9 and 29. Those works report that the best superconducting properties were achieved using a crystallization temperature ($T_{crys}$) of 780 °C and an oxygen partial pressure ($pO_2$) of 200 ppm for

YBCO + 12% BHO while for GdBCO + 12% BHO the $T_{crys}$ was 810 °C and the $pO_2$ 50 ppm. One should nevertheless take into account that the synthesis of GdBCO films (or other REBCO compounds with larger ion size) is very difficult, and the use of mixed-RE compounds could increase the reproducibility in the preparation of high-quality films significantly. The optimization consisted of varying the $T_{crys}$ and $pO_2$ for each stoichiometry looking for the best possible $J_c^{sf}$ at 77 K and finding, therefore, the optimum $T_{crys}$ or $pO_2$. Fig. 1 shows the dependency of $J_c^{sf}$ at 77 K with the optimum $T_{crys}$ (a) and $pO_2$ (b) for $x = 0$, 0.5, and 1. In the investigated ranges, the dependencies are much smoother in the case of $Y_{0.5}Gd_{0.5}BCO$ + 12% BHO films than for YBCO + 12% BHO or GdBCO + 12% BHO films. Especially dramatic is the decay (more than 50%) of $J_c^{sf}$ when moving away from the optimum condition in the GdBCO + 12% BHO case. The optimum window is reached only within a margin of 10 °C and 50 ppm (the lower limit of our experimental range). Instead, in the case of the $Y_{0.5}Gd_{0.5}BCO$ + 12% BHO films, it is possible to move the $T_{crys}$ and $pO_2$ in a large range of more than 60 °C and 150 ppm obtaining films with $J_c^{sf}$ at 77 K larger than 3 MA cm$^{-2}$ (also ~50% of decay with respect to the highest value). This comparison clearly demonstrates that the processing windows for the mixed-RE films are much larger than in the case of the single-RE films. This large room gives a lot of freedom to select the most convenient processing parameters to adapt to different substrates which is very important for the industrial production of CCs.

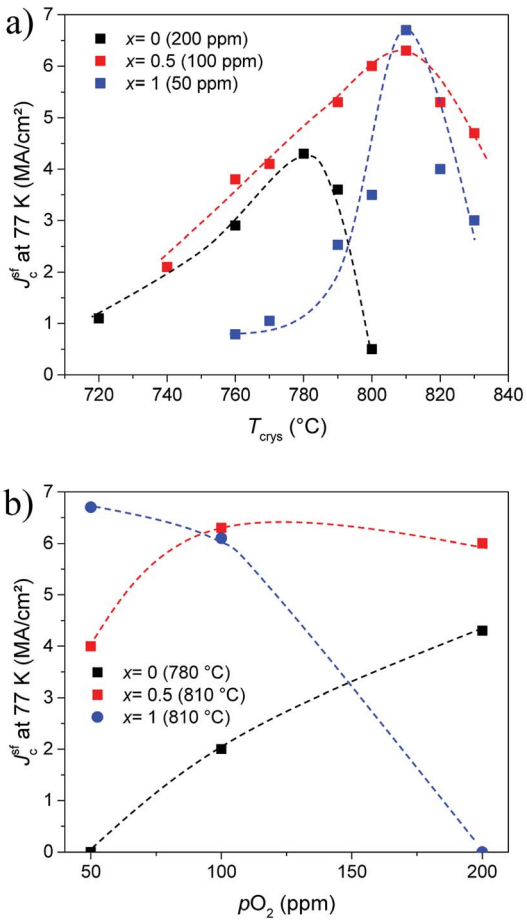


Fig. 1 Dependence of $J_c^{sf}$ at 77 K on (a) $T_{crys}$ and (b) $pO_2$ for $Y_{1-x}Gd_xBa_2Cu_3O_7$ + 12% $BaHfO_3$ films with $x = 0$, 0.5, and 1 at the optimum value of the respective other parameter.

Table 1 Optimized crystallization temperature ($T_{crys}$) and oxygen partial pressure ($pO_2$) depending on Gd content $x$ in $Y_{1-x}Gd_xBa_2Cu_3O_{7-\delta}$ + 12% BHO nanocomposite films

| $x$ | Optimized $T_{crys}$ (°C) | Optimized $pO_2$ (ppm) |
|---|---|---|
| 0 | 780 | 200 |
| 0.33 | 790 | 150 |
| 0.5 | 810 | 100 |
| 0.66 | 810 | 75 |
| 1 | 810 | 50 |

As shown in Table 1, the optimum crystallization temperature is progressively increasing and the optimal oxygen partial pressure decreasing and approaching the optimum values for the GdBCO + 12% BHO films for higher values of $x$ (Table 1). It can not be excluded at this stage that slightly higher $J_c$ values for YBCO + 12% BHO at $pO_2$ > 200 ppm are possible. This shall be determined in on-going investigations.

After the optimization had been completed for each stoichiometry, only the optimized films were used for the rest of the investigations shown in the following.

### 3.2 Superconducting properties

Fig. 2 shows clearly systematic trends with Gd content $x$. $T_c$ increases almost linearly from ~90 K for the YBCO + BHO films to ~94 K for the GdBCO + BHO films. A similar trend is noticed for $J_c^{sf}$ at 77 K. These values increase monotonously with $x$ but in a more irregular way than $T_c$. $J_c^{sf}$ at 77 K of $Y_{0.5}Gd_{0.5}BCO$ + 12% BHO and $Y_{0.33}Gd_{0.66}BCO$ + 12% BHO are higher than expected from the $T_c$ trend. The $J_c^{sf}$ values at 77 K for films with $x$ > 0.5 are larger than 7 MA cm$^{-2}$, which is comparable to values of GdBCO + 12% BHO films reported recently[9] and are the highest values ever reported for CSD-grown YGBCO films and among the highest for REBCO. Finally, the $x$ dependence of the irreversibility field ($B_{irr}\|c$) at 77 K increases also monotonically with Gd content. The highest value is reached for the GdBCO + 12% BHO film at 9.9 T while the value for the nearest YGBCO + 12BHO films is 9.4 T for $x = 0.66$. This trend in $B_{irr}$ (77 K) is directly related with the variation in $T_c$. Also the $J_c^{sf}$ values at 77 K are strongly influenced by $T_c$, and this is why the highest $J_c^{sf}$ is found in the GdBCO + 12% BHO film which also has the highest $T_c$.

### 3.3 Structure and surface morphology

The $\theta$–$2\theta$ patterns of the YGBCO + 12% BHO films grown at their optimum processing parameters, Fig. 3, present similar patterns with only (00$l$)YGBCO reflections besides the STO substrate reflections and clear signs of BHO. In some of the patterns, weak reflections of $(YGd)_2O_3$ are noticed. However, no signs of $a$-$b$-oriented or other misoriented grains can be observed.

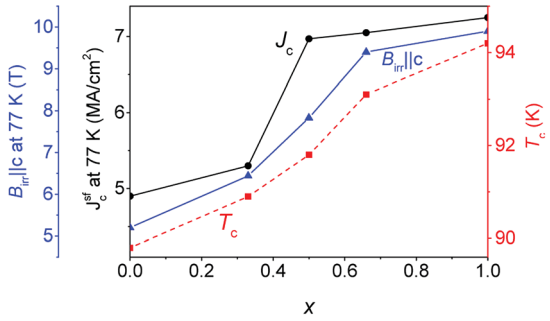


Fig. 2 Dependence of the transport $J_c^{sf}$ at 77 K (black curve), $T_c$ (red curve) and irreversibility field ($B_{irr}||c$) at 77 K (blue curve) on the amount of Gd present in the YGBCO + 12% BHO films.

Also sharp in-plane and out-of-plane orientation is observed for these films, as shown in Fig. 4 for the $Y_{0.33}Gd_{0.66}BCO$ + 12% BHO film exemplarily. The (102)YGBCO phi-scan (Fig. 4a) shows 4-fold symmetry and sharp peaks with FWHM values $\Delta\phi$ of 1.09°. The (005)YGBCO rocking curve (Fig. 4b) has a FWHM, $\Delta\omega$, of 0.23°, indicating fully epitaxial growth with cube-on-cube relationship. The texture quality is comparable to the values obtained in our previous work for the GdBCO + 12% BHO films.[9]

The absence of misoriented grains in optimized films as deduced from XRD is confirmed by the surface morphology in SEM pictures, Fig. 5. Even though the films are in general very dense and homogenous with only superficial indentations, certain systematic differences in the morphology of the films are noticeable. With Gd content $x$, the films become denser (less porous) and smoother. This can be attributed to the increase of the optimum $T_{crys}$ for higher values of $x$ (Section 3.1) which makes the sintering process more effective, and, as a consequence of that, denser films can be obtained. This can explain the fact that $J_c^{sf}$ at 77 K of the $Y_{0.5}Gd_{0.5}BCO$ + 12% BHO and $Y_{0.33}Gd_{0.66}BCO$ + 12% BHO films are higher than expected from a linear $T_c$ behavior.

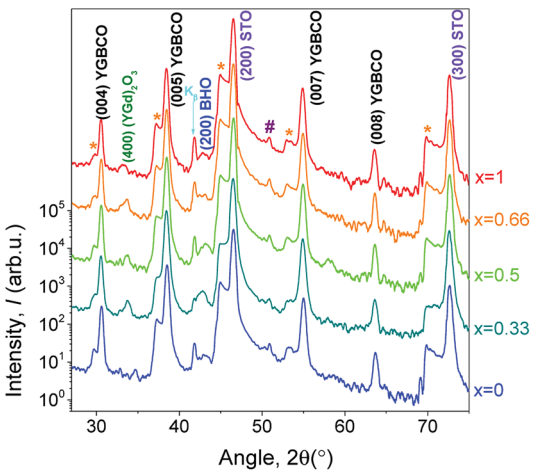


Fig. 3 XRD patterns of $Y_{1-x}Gd_xBa_2Cu_3O_{7-\delta}$ + 12% BHO films grown with optimized processing parameters. The peaks marked with * and # come from the experimental setup ($K_\beta$ filter and X-ray source, respectively).

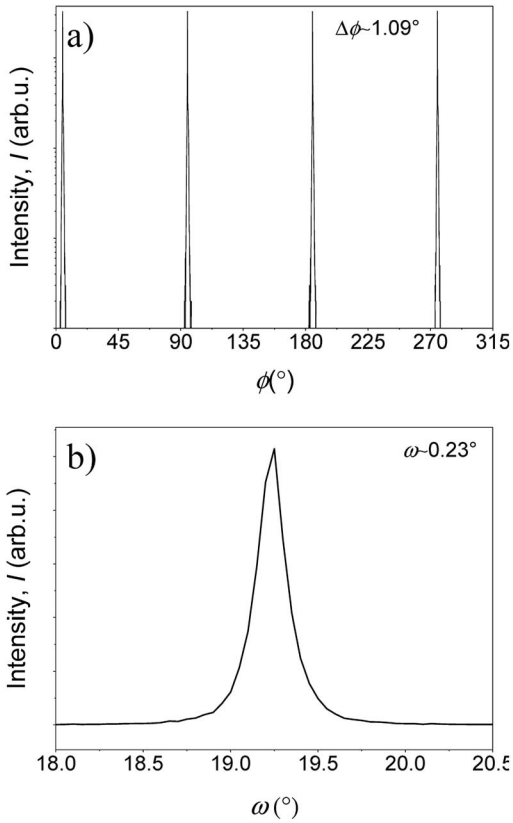


Fig. 4 Texture quality of an optimized $Y_{0.33}Gd_{0.66}BCO$ + 12% BHO film showing (a) the $\phi$-scan of (102)YGBCO and (b) the (005)YGBCO rocking curve.

### 3.4 In-field electrical transport properties

Fig. 6 illustrates the strong improvement in $J_c(B)$ (a) and pinning force density, $F_p(B)$ (b) for the optimized YGBCO + 12% BHO nanocomposite films in comparison with pristine YBCO and $Y_{0.5}Gd_{0.5}BCO$ films in almost the entire investigated magnetic field range at 77 K. Similar $J_c^{sf}$ at 77 K values and $J_c(B)$ dependences with the magnetic field were reported for YBCO + 10% BZO films with similar thickness.[27,28]

Large maximum pinning force densities, $F_{pmax}$, at 77 K were reached: ~11 GN m$^{-3}$ (1.6 T) for the films $Y_{0.5}Gd_{0.5}BCO$ + 12% BHO and $Y_{0.33}Gd_{0.66}BCO$ + 12% BHO. These values are not as high as in the case of the GdBCO + 12% BHO film but the improvement with respect to the YBCO + 12% BHO is still remarkable.

The YGBCO + 12% BHO films show higher self-field and in-field values of $J_c$ and $F_{pmax}$ at 77 K than the YBCO + 12% BHO films but still the GdBCO + 12% BHO film has larger values than those. As mentioned before, this is due to the larger irreversibility field at 77 K in the case of GdBCO + 12% BHO films, and the properties will be very influenced by the differences in $T_c$ at temperatures close to $T_c$. However, this behavior could be different at lower temperatures where $T_c$ has not such a large influence any more. Measurements at these temperatures in future investigations would help disentangle $T_c$ and RE mixing effects.

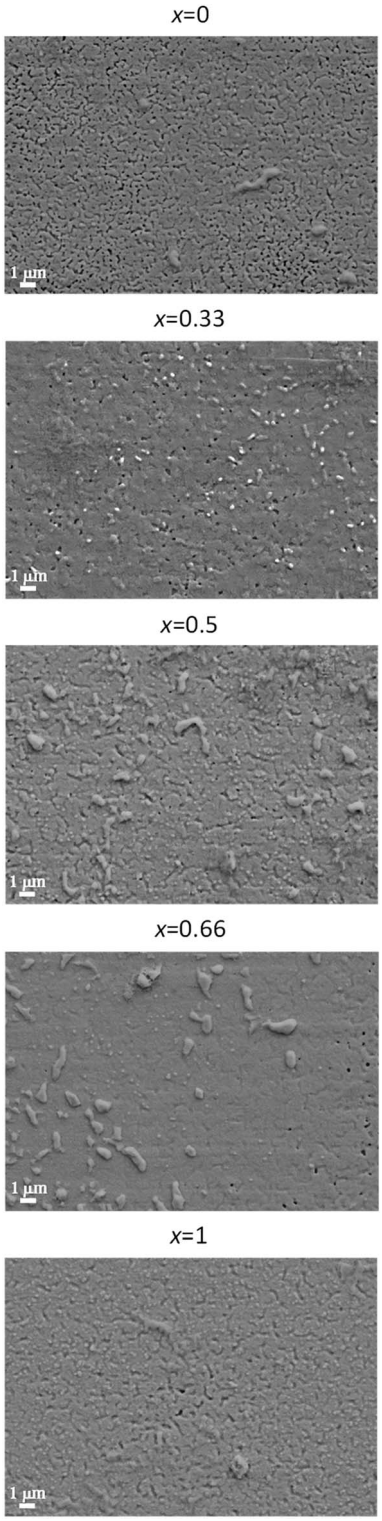


Fig. 5 Surface morphology of YGBCO + 12% BHO films with different Gd content $x$ grown at optimized processing parameters observed *via* SEM imaging.

In summary, at 77 K the best option is to use GdBCO films (or, in general, REBCO films with high $T_c$) if one can produce high-quality GdBCO films in a reproducible way. However, at lower temperatures, where the influence of $T_c$ is less severe, the use of YGBCO films or other mixed-RE compounds will be much more interesting since the effects of the mixing, in terms of pinning properties, will not be eclipsed by the $T_c$ difference. Therefore, in order to study the full potential of CSD-grown YGBCO + 12% BHO films and to make a fair comparison with the GdBCO + 12% BHO films, lower temperature measurements are needed, which are planned for follow-up studies.

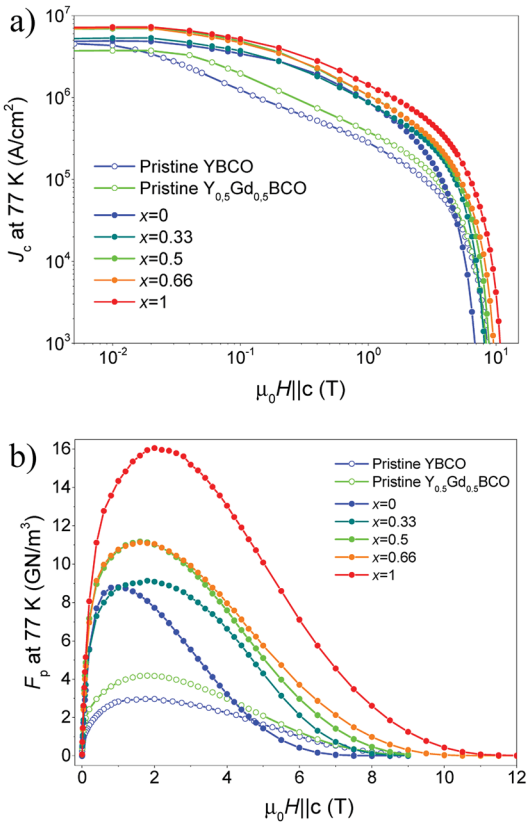


Fig. 6 Transport measurements on optimized YGBCO + 12% BHO films in comparison with pristine YBCO and $Y_{0.5}Gd_{0.5}BCO$ films showing (a) the $J_c$ dependence with the magnetic field at 77 K and (b) pinning force density ($F_p$) at 77 K.

## 4. Conclusions

We have studied the simultaneous effect of mixed rare earth and nanoparticle inclusion on superconducting transport properties at 77 K in $Y_{1-x}Gd_xBa_2Cu_3O_{7-\delta}$–$BaHfO_3$ films with Gd content $x$. Each particular composition presents a different set of optimized processing parameters with $T_{crys}$ between 780 and 810 °C and $pO_2$ between 50 and 200 ppm. However, we demonstrated that the window of useful processing parameters is much wider in the case of YGBCO + 12% BHO films with $x \neq \{0, 1\}$ which is very beneficial for the industrial production of CCs. The analysis of the superconducting properties revealed that the $T_c$ varies almost linearly with Gd content, and this has a large influence on $B_{irr}$, $F_{pmax}$ and $J_c^{sf}$ at 77 K. The values for YGBCO + 12% BHO lie between the values of YBCO + 12% BHO and GdBCO + 12% BHO films. The $J_c$ and $F_p$ values for the YGBCO + 12% BHO films are superior to the case of the YBCO +

12% BHO films but lower than for the GdBCO + 12% BHO films. Therefore, we can conclude that at 77 K the value of $T_c$ and, hence, the value of the irreversibility field have a much larger influence than a possible improvement in the pinning properties due to mixed RE. Therefore, it would be better to use REBCO films with high $T_c$ values at 77 K. However, this is not always possible because the synthesis of these high-$T_c$ compounds with large RE ion size is more difficult and, therefore, less reproducible. So, the use of YGBCO + 12% BHO films is still advantageous even for applications at 77 K because they combine production in a very reproducible way with improved superconducting properties.

## Conflicts of interest

There are no conflicts to declare.

## Acknowledgements

The research leading to these results received funding from EUROTAPES, a collaborative project funded by the European Union's Seventh Framework Program (FP7/2007–2013) under grant agreement no. NMP-LA-2012-280 432. We gratefully acknowledge funding the Bruker D8 through the Helmholtz Energy Materials Characterization Platform (HEMCP) initiated by the Helmholtz Association. We also acknowledge the support by Deutsche Forschungsgemeinschaft and Open Access Publishing Fund of Karlsruhe Institute of Technology.

## Notes and references

1 Y. Iijima, N. Tanabe, Y. Ikeno and O. Kohno, *Phys. C*, 1991, **185–189**, 1959–1960.
2 K. Hasegawa, K. Fujino, H. Mukai, M. Konishi, K. Sato, S. Honjo, Y. Sato, H. Ishii and Y. Iwata, *Appl. Supercond.*, 1996, **4**, 487–493.
3 A. Goyal, M. P. Paranthaman and U. Schoop, *MRS Bull.*, 2004, **29**, 552–561.
4 J.-H. Lee, H. Lee, J.-W. Lee, S.-M. Choi, S.-I. Yoo and S.-H. Moon, *Supercond. Sci. Technol.*, 2014, **27**, 44018.
5 M. Murakami, N. Sakai, T. Higuchi and S. I. Yoo, *Supercond. Sci. Technol.*, 1996, **9**, 1015–1032.
6 Y. Yoshida, T. Ozaki, Y. Ichino, Y. Takai, K. Matsumoto, A. Ichinose, M. Mukaida and S. Horii, *Phys. C*, 2008, **468**, 1606–1610.
7 S. H. Wee, A. Goyal, P. M. Martin and L. Heatherly, *Supercond. Sci. Technol.*, 2006, **19**, 865–868.
8 P. Cayado, B. Mundet, H. Eloussifi, F. Vallés, M. Coll, S. Ricart, J. Gázquez, A. Palau, P. Roura, J. Farjas, T. Puig and X. Obradors, *Supercond. Sci. Technol.*, 2017, **30**, 125010.
9 P. Cayado, M. Erbe, S. Kauffmann-Weiss, C. Bühler, A. Jung, J. Hänisch and B. Holzapfel, *Supercond. Sci. Technol.*, 2017, **30**, 094007.
10 C. Andreouli and A. Tsetsekou, *Phys. C*, 1997, **291**, 274–286.
11 J. L. MacManus-Driscoll, J. A. Alonso, P. C. Wang, T. H. Geballe and J. C. Bravman, *Phys. C*, 1994, **232**, 288–308.
12 J. L. MacManus-Driscoll, S. R. Foltyn, Q. X. Jia, H. Wang, A. Serquis, B. Maiorov, L. Civale, Y. Lin, M. E. Hawley, M. P. Maley and D. E. Peterson, *Appl. Phys. Lett.*, 2004, **84**, 5329–5331.
13 J. L. MacManus-Driscoll, S. R. Foltyn, Q. X. Jia, H. Wang, A. Serquis, B. Maiorov, L. Civale, Y. Lin, M. E. Hawley, M. P. Maley and D. E. Peterson, *Appl. Phys. Lett.*, 2005, **86**, 32505.
14 M. S. Islam and R. C. Baetzold, *Phys. Rev. B: Condens. Matter Mater. Phys.*, 1989, **40**, 10926–10935.
15 J. L. Macmanus-Driscoll, *Adv. Mater.*, 1997, **9**, 457–473.
16 S. H. Wee, A. Goyal, E. D. Specht, C. Cantoni, Y. L. Zuev, V. Selvamanickam and S. Cook, *Phys. Rev. B: Condens. Matter Mater. Phys.*, 2011, **83**, 224520.
17 M. Miura, T. Kato, M. Yoshizumi, Y. Yamada, T. Izumi, T. Hirayama and Y. Shiohara, *Appl. Phys. Express*, 2009, **2**, 23002.
18 V. Selvamanickam, Y. Chen, Y. Zhang, A. Guevara, T. Shi, Y. Yao, G. Majkic, C. Lei, E. Galtsyan and D. J. Miller, *Supercond. Sci. Technol.*, 2012, **25**, 45012.
19 M. Irjala, H. Huhtinen, P. Paturi, A. Kumar, V. P. S. Awana, A. V. Narlikar and R. Laiho, *J. Phys.: Conf. Ser.*, 2009, **153**, 12014.
20 K. Kinoshita, A. Matsuda, H. Shibata, T. Ishii, T. Watanabe and T. Yamada, *Jpn. J. Appl. Phys.*, 1988, **27**, L1642–L1645.
21 H. H. Wen, Z. X. Zhao, R. L. Wang, H. C. Li and B. Yin, *Phys. C*, 1996, **262**, 81–88.
22 H. Jian, D. Shao, Z. Yang, X. Zhu and Y. Sun, *Phys. C*, 2013, **88**, 39–45.
23 M. Muralidhar and M. Murakami, *Supercond. Sci. Technol.*, 2000, **13**, 1315–1321.
24 C. Cai, J. Hänisch, T. Gemming and B. Holzapfel, *IEEE Trans. Appl. Supercond.*, 2005, **15**, 3738–3741.
25 *Studies of high temperature superconductors*, ed. A. V. Narlikar, Nova Science Publishers, 2006, vol. 49.
26 Y. Li and Z.-X. Zhao, *Phys. C*, 2001, **351**, 1–4.
27 J. Gutiérrez, A. Llordés, J. Gázquez, M. Gibert, N. Romà, S. Ricart, A. Pomar, F. Sandiumenge, N. Mestres, T. Puig and X. Obradors, *Nat. Mater.*, 2007, **6**, 367–373.
28 A. Llordés, A. Palau, J. Gázquez, M. Coll, R. M. Vlad, A. Pomar, J. Arbiol, R. Guzmán, S. Ye, V. Rouco, F. Sandiumenge, S. Ricart, T. Puig, M. Varela, D. Chateigner, J. Vanacken, J. Gutiérrez, V. V. Moshchalkov, G. Deutscher, C. Magén and X. Obradors, *Nat. Mater.*, 2012, **11**, 329–336.
29 M. Erbe, J. Hänisch, R. Hühne, T. Freudenberg, A. Kirchner, L. Molina-Luna, C. Damm, G. Van Tendeloo, S. Kaskel, L. Schultz and B. Holzapfel, *Supercond. Sci. Technol.*, 2015, **28**, 114002.
30 P. Cayado, K. De Keukeleere, A. Garzón, L. Perez-Mirabet, A. Meledin, J. De Roo, F. Vallés, B. Mundet, H. Rijckaert, G. Pollefeyt, M. Coll, S. Ricart, A. Palau, J. Gázquez, J. Ros, G. Van Tendeloo, I. Van Driessche, T. Puig and X. Obradors, *Supercond. Sci. Technol.*, 2015, **28**, 124007.
31 K. De Keukeleere, P. Cayado, A. Meledin, F. Vallès, J. De Roo, H. Rijckaert, G. Pollefeyt, E. Bruneel, A. Palau, M. Coll,

S. Ricart, G. Van Tendeloo, T. Puig, X. Obradors and I. Van Driessche, *Adv. Electron. Mater.*, 2016, **2**, 1600161.

32 S. Engel, T. Thersleff, R. Hühne, L. Schultz and B. Holzapfel, *Appl. Phys. Lett.*, 2007, **90**, 102505.

33 S. Lu, L. Liu, W. Wang, X. Wu, Y. Yao, B. Wang and Y. Li, *J. Supercond. Novel Magn.*, 2018, **31**, 7–11.

34 L. Liu, W. Wang, T. Zheng, S. Liu, W. Wang and Y. Li, *J. Supercond. Novel Magn.*, 2018, **31**, 1–7.

35 X. Obradors and T. Puig, *Supercond. Sci. Technol.*, 2014, **27**, 44003.

36 X. Obradors, T. Puig, A. Pomar, F. Sandiumenge, S. Piñol, N. Mestres, O. Castaño, M. Coll, A. Cavallaro, A. Palau, J. Gázquez, J. C. González, J. Gutiérrez, N. Romà, S. Ricart, J. M. Moretó, M. D. Rossell and G. van Tendeloo, *Supercond. Sci. Technol.*, 2004, **17**, 1055–1064.

37 X. Obradors, T. Puig, A. Pomar, F. Sandiumenge, N. Mestres, M. Coll, A. Cavallaro, N. Romà, J. Gázquez, J. C. González, O. Castaño, J. Gutiérrez, A. Palau, K. Zalamova, S. Morlens, A. Hassini, M. Gibert, S. Ricart, J. M. Moretó, S. Piñol, D. Isfort and J. Bock, *Supercond. Sci. Technol.*, 2006, **19**, S13–S26.

38 T. Izumi, M. Yoshizumi, J. Matsuda, K. Nakaoka, Y. Kitoh, Y. Sutoh, T. Nakanishi, A. Nakai, K. Suzuki, Y. Yamada, A. Yajima, T. Saitoh and Y. Shiohara, *Phys. C*, 2007, **463**, 510–514.

39 A. Gupta, R. Jagannathan, E. I. Cooper, E. A. Giess, J. I. Landman and B. W. Hussey, *Appl. Phys. Lett.*, 1988, **52**, 2077–2079.

40 M. Erbe, J. Hänisch, T. Freudenberg, A. Kirchner, I. Mönch, S. Kaskel, L. Schultz and B. Holzapfel, *J. Mater. Chem. A*, 2014, **2**, 4932.